# Effects of Ag addition on the Precipitation Hardening Behaviours and Corrosion properties of Al-Mg-Si Alloy

*Ya-ya Zheng[1,2], Bing-hui Luo[1,*], Chuan He[1], Zhi-wei Ren[1], Yuan Yin[1]*

[1] College of Materials Science and Engineering, Central South University, Changsha 410083, China；
[2] Key Laboratory of Safety Design and Reliability Technology for Engineering Vehicle, Changsha University of Science and Technology, Changsha 410114, China
[*]E-mail: luobinghui@csu.edu.cn

The effects of Ag on the microstructure, dynamic precipitation and corrosion properties of Ag-Mg-Si alloys were investigated, by using scanning electron microscopy (SEM), transmission electron microscopy (TEM), potentiodynamic polarization measurements and differential scanning calorimetry (DSC). The results show that with the increase in Ag content, the alloys peak hardness, the aging hardening speed and the electrical conductivity increase, but the softening speed decreases. The addition of Ag significantly accelerates the kinetic process of aging precipitation of Ag-Mg-Si alloy, improves the density and the thermodynamic stability of β" phase ($Mg_5Si_6$) and reduces the precipitation activation energy of the β" and β′ phase. The alloy without Ag exhibits severe local corrosion and intergranular corrosion; the alloy with 0.3 wt.% Ag exists fewer grain boundary precipitates and exhibits a slight intergranular corrosion (IGC). The addition of excess Ag leads to the increase in the corrosion sensitivity.

## 1. INTRODUCTION

Al-Mg-Si alloys have been widely used in automobiles to improve fuel economy and reduce vehicle weight due to their desirable combination of high strength and low density [1]. The precipitation sequence of Al-Mg-Si alloy is generally expressed as: SSS (supersaturated solid solution) → needle-like β" → rod-like β′ → β/Si.[2-3] β" is the main strengthen phase of Al-Mg-Si. There is some elemental Si phase, when the Si content exceeds a certain amount [4-6].

Microalloying is an important development direction to improve the performance of aluminum alloys. The addition of microalloying elements can greatly affect the aging precipitation behavior of Al-Mg-Si alloy, and adjust the properties of the alloys. After Cu is added, the precipitation sequence of the

alloy is: SSSS → GP-zones → needle-like β″ → lath-like Q′ / rod-like β′ → Q+β, and the aged hardening response of Al-0.72Mg-1.2Si alloy can be significantly improved, and the alloy peak-aging platform is prolonged [7]. Gaber showed that the precipitation of Q' phase is controlled by the diffusion of Mg, Si and Cu. The addition of excess Cu can inhibit the precipitation of β' [8]. Kim indicated that Cu can low the formation temperature of nanoclusters of Al-Mg-Si alloy, and increase the effect of natural aging [9]. Yuan showed that adding a small amount of Zr into the Al-Mg-Si alloy has no effect on the precipitation sequence, but the tensile strength and heat resistance of the alloy can be improved [10]. Ding indicated that in the Al-Mg-Si alloy with minor Cu, excess Si has higher peak aging hardness and mechanical properties than that of the alloy with excess Mg, but the corrosion sensitivity is also higher [11]. Marioara showed that the addition of minor Ag can increases the precipitation speed of β″ and improves the hardness of the Al-Mg-Si alloy [12]. Nakamura showed that after adding a large amount of Ag, the Ag atom can replace part of the Mg atom, leading to the appearance of β' phase with hexagonal unit cell composed of Mg, Si and Ag [13]. Zheng showed that excess Si can increase responsive speed of the precipitation of β″ phase, but reduce the IGC resistance of the alloy [1].

For high-performance Al-Mg-Si alloys, it is necessary to have both high mechanical properties and excellent corrosion resistances to reduce the failure during service. The addition of Ag is an effectively approach to improve the overall performance to extend service life of the Al-Mg-Si alloy [14-15]. A minor addition of Ag can significantly change the microstructure and the properties of the alloy, such as forming Ag-contained phase, accelerating the aging precipitation process, and improving the mechanical properties and corrosion resistance [16-17]. In this paper, efforts were focused on investigating the effect of Ag on the aging precipitation kinetics and corrosion performances, to provide a theoretical basis for further optimizing the properties of Al-Mg-Si alloys, and broadening the application of Al-Mg-Si alloys.

## 2. EXPERIMENTAL PROCEDURES

The analysed chemical compositions of the three investigated alloys are shown in Table 1. Hardness and electrical conductivity were tested by HAZ-5 Vickers hardness tester and 7501 conductivity meter respectively to characterize the hardening behavior and electric conductivity change of the alloy during artificial aging. The solid solution stated sample was used to thermal analysis on a SP type DSC under an argon atmosphere. Heating temperature range from 50℃ to 500℃ and heating rate is 10℃/min. The test results are deducted from the noise floor with high purity aluminum as a reference.

These samples are subjected sequently to the following heat treatment: 500℃/36h for homogenization, hot rolled, cold rolled, solid solution treatment at 520℃ for 2h, water quenching at room temperature and aging at 170℃.

**Table 1.** Analysed chemical composition of the alloys

| Alloy No. | Mass fraction wt.% | | | | | | | Al |
|---|---|---|---|---|---|---|---|---|
| | Mg | Si | Mn | Zr | Cr | Ti | Ag | |
| Alloy A | 1.81 | 2.10 | 0.44 | 0.15 | 0.20 | 0.50 | 0 | Bal. |
| Alloy B | 1.80 | 2.10 | 0.45 | 0.16 | 0.21 | 0.50 | 0.31 | Bal. |
| Alloy C | 1.79 | 2.09 | 0.45 | 0.15 | 0.20 | 0.50 | 0.59 | Bal. |

The polarization curve is measured using a typical three-electrode system: the reference electrode is a saturated calomel electrode (SCE), the auxiliary electrode is a platinum plate electrode, and the working electrode is the sample to be tested. The test face with a size of 10 mm length × 10 mm width × 8 mm were measured by using a EG&G Model 273 Galvanostat/Potentiostat in the potential range from -1.5 to -0.2 V vs open circuit potential to estimate the reactions between the anodic and cathodic partial electrode, and the scanning rate is 2 mV/s. The corrosion current density ($i_{corr}$) and corrosion potentials ($E_{corr}$) were obtained with NOVA software. The IGC performance test selects the T6 state sample. IGC was carried out in 5% NaCl aqueous solution. The morphology of the samples after IGC test was observed by XJG-OS metallographic microscope and a scanning electron microscope. The transmission samples were thin disk prepared in a twin-jet electro polishing unit with a solution of 80% methanol and 20% nitric acid with 22V in -25°C, and the microstructure of the alloy were observed by TECNAI F20. Analysis of the HRTEM images was performed using the Gatan DigitalMicrograph™ software and the NIH ImageJ software.

## 3. RESULTS AND DISCUSSION

### 3.1. Effect of Ag Content on A1-Mg-Si Ageing Behavior

Fig.1 shows the evolutions of hardness and the electric conductivity of the three alloys artificial ageing at 170 °C. The tendencies of the hardness and the electric conductivity curve of the three alloys are quite similar, featuring a rapid rise to peak value at first, and remained constant for a longer time, then followed with a slow decreasing tendency. The hardness value of the three alloys at the solid solution state are all about 89 HV, indicating that the hardness difference caused by Ag content are not obvious. The increase in Ag content enhances both the age-hardening rate and hardness peak value, and also slows the decreasing rate of the hardness. Alloy C can reach the peak hardness of 131 HV after aging for 6h, while the alloy A and B need 9h and 8h aging time respectively to reach the corresponding peak hardness of 120 and 126HV. From previous studies described in References [9,11], peak hardness is mainly caused by the presence of β″ phase ($Mg_5Si_6$) and β′ precipitates, and the increased Ag content could increase the density of these strengthening phases. After 24h aging (at the over aging state), the hardness of alloy A, B and C decreases to 106, 112 and114 HV respectively, compared with the peak hardness, the hardness decreases by 13, 12 and 16 HV respectively, which means that increasing the Ag content to 0.6 wt. % can result in more hardness decrease.

As well, the Ag content has little impact on the electric conductivity of these alloys at solid

solution state, which means that the increase in Ag contents has no effect on the lattice distortion of Al matrix. It is worth noting that increasing the Ag content to 0.6wt.% is not beneficial to further enhance of the electric conductivity. The electric conductivity of the alloy with 0.3wt.%Ag is larger than that of the alloy C with 0.6%Ag at peak aging state. Fig. 1(b) illustrates the effect of Ag content on the relationship between the hardness and the electric conductivity. The alloy C has the peak hardness of 131HV and the electric conductivity of 45.1% IACS, The alloy B has the peak hardness of 126HV and the electrical conductivity of 45.7% IACS, which indicates that excessive addition of Ag is not conducive to the improvement of comprehensive properties of the alloy.
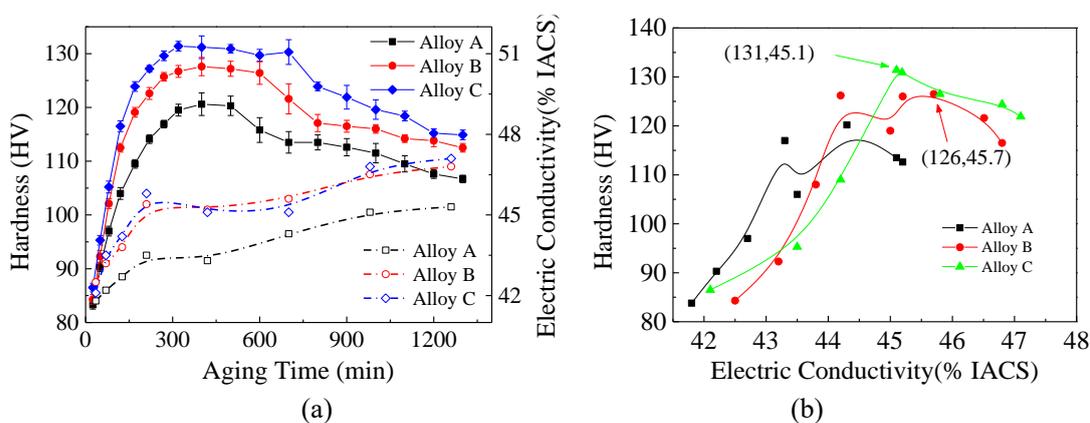


**Figure 1.** Relationships between hardness, electric conductivity of the samples and aging time: (a) Vickers hardness curves; (b) the hardness as a function of the electrical conductivity

## 3.2 IGC

Fig.2 shows the morphology of corrosion surface and cross-sectional of the three alloys after immersion for 12 hours in 3.5wt.% NaCl solution. All the alloys exhibit various degrees of IGC. The corrosion degree is determined by the maximum corrosion depth. Alloy A appears serious local corrosion and IGC (Fig. 2(a)), and some grains are stripped from matrix (Fig. 2(d)). The maximum corrosion depth reached 79 μm. Alloy B exhibits typical IGC (Fig. 2b) with the maximum corrosion depth of 46 μm (Fig. 6d), and the surface grains are relatively intact. The maximum corrosion depth of Alloy C is 53 μm (Fig. 6f), which increase slightly compared to Alloy B. Alloy A exhibited the highest IGC sensitivity among the three alloys, followed by Alloy C. The aforementioned results with respect to corrosion behavior are related to influence of the electrochemical property of the second phase, the continuity degree of grain boundary precipitates, and the effectiveness of the corrosion resistance of the alloy oxide film [18].
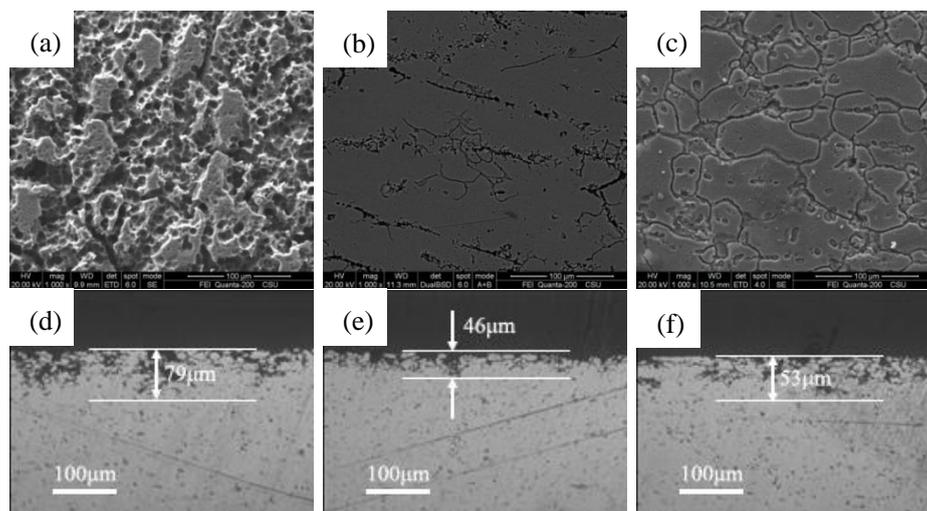
**Figure 2.** Surface morphologies and corresponding cross-sections of the corroded alloys with different Ag contents: (a,d) alloy A, (b,e) alloy B, and (c,f) alloy C.

*3.3 Potentiodynamic Polarization Tests*

Fig.3 shows the potentiodynamic polarization results in 3.5wt.% NaCl aqueous solution at room temperature 25℃ ±3℃. The electrochemical parameters are shown in Table 2 obtained by the polarization curves. $E_{corr}$, $E_{pit}$, $I_{corr}$ is the corrosion potential, pitting potential and corrosion current density respectively. The polarization curves of the examined alloys have similar shapes, with standard Tafel interval, passivation platforms, and transpassive interval. The corrosion resistances of the alloys are mainly due to the formation of a protective passive oxide film on the surface. The existence of the passivation platform results from oxide film with the property of effectively preventing the Cl$^-$ ions from penetrating into the Al matrix [19]. The oxide film includes the outer layer composed of amorphous hydrate and amorphous alloy, and the transition layer (dense inner layer) between the outer layer and the metal matrix. The outer layer with lower physical and chemical stability, may consist of $Al_2O_3$ mixture and hydrated $Al_2O_3$, such as Al $(OH)_3$ and AlOOH. The transition layer is mainly composed of $Al_2O_3$ and a small amount of hydrated alumina [20]. Due to the second phase, the outer layer of the oxide film inevitably exist flaw, where corrosion begins. Even in the region where the oxide film is relatively intact [21-22]. A schematic of the corrosion processes that occurring within the oxide film is presented in Fig. 3(b).

The reaction (1) describes the Al as interstitial atoms, pass through the oxide layer into solution (reaction 2), and produce a vacancy in the metal layer. The reaction (3) indicates that the oxygen atom diffuses into the metal layer and forms aluminum oxide, which makes the oxide film grow into the Al matrix, and produces an oxygen atom vacancy in the oxide film.
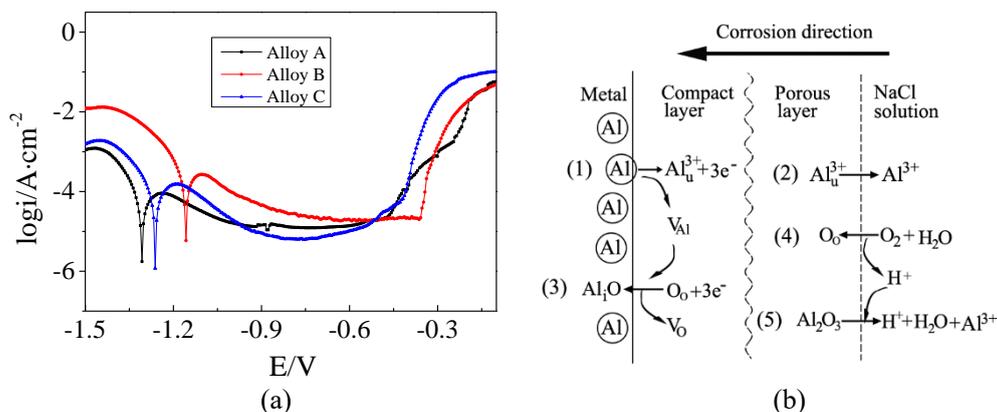
**Figure 3.** Polarization curves of the tested alloys and corrosion processes occurring in the oxide film. (a) Polarization curves of the tested alloys; (b) Physicochemical processes occurring in the oxide film. $Al_u^{3+}$: aluminum cation in a instability cation position. $V_{Al}$: aluminum vacancy at metal phase. $V_o$: oxygen vacancy at compact layer. $O_o$: oxygen ion in anion state

**Table 2**. Polarization curve related parameters determined by the Tafel extrapolation method.

| Sample | $E_{corr}$ (V vs SCE) | $E_{pit}$ (mV vs SCE) | $i_{corr}$ ($\mu A$ cm$^{-2}$) | $\beta_a$ (mV/dec) | $\beta_c$ (mV/dec) |
|--------|------------------------|------------------------|----------------------------------|---------------------|---------------------|
| Alloy A | -1.32 | -413±3 | 245±11 | 85 | 124 |
| Alloy B | -1.13 | -352±3 | 168±9 | 71 | 131 |
| Alloy C | -1.25 | -409±3 | 212±5 | 79 | 126 |

Note:$E_{corr}$ is the self-corrosion potential, $I_{corr}$ is the corrosion current density, and $E_{pit}$ is the pitting potential

The oxygen atom vacancies are occupied by the dissolved oxygen from the water (reaction (4)), The $H^+$ produced by reaction (4) causes localized acidification at the oxide film/solution interface, and promotes the dissolution of the oxide film (reaction (5)). As shown in Table 2, with the increasing Ag content, the corrosion current density of the alloy decreases firstly and then increases. When the content of Ag is 0.3 wt.%, the corrosion resistance of the alloy is the best. In addition, the various values of $\beta_a$ and $\beta_c$ indicating that the corrosion rate of the alloy may be concurrently influenced by the electrochemical activity of cathodic and the anode phase.

### 3.4 Effect of Ag content on the Microstructure of A1-Mg-Si alloy

The TEM images of the three Al-Mg-Si alloys in peak-aging condition are shown in Fig.4. The experiment was carried out with the electron beam parallel to the $[001]_{Al}$ axis. As clearly observed, there are many needle-like phases in these three alloys, and the density of these phase increases with the increase in Ag content, which causes improvement of the hardness [7,12]. In order to further analyze and confirm the structure of these needle-like phases, The Fast Fourier transform (FFT) was applied to the high-resolution TEM (HRTEM) image regarding the cross-section of the representative needle-like phases shown in Fig. 4(d, e, f). The perceived phases are supposed to be polygonal and can be identified as a monoclinic system. The lattice parameters are calculated: a=1.51 nm, c=0.67 nm, β=105.3°. It can be deduced that these needle-like phases are β" phase ($Mg_5Si_6$) [1,4].

The type and distribution of grain boundary precipitates play an important role on corrosion properties. Fig. 4 (g~i) shows the effects of Ag content on the grain boundary precipitates. All of the three alloys exist short rod-like precipitates intermittently distributing at the grain boundary, but the PFZs are not obvious, indicating that the alloys may have better corrosion resistances than that of the traditional Al-Mg-Si alloy. Among the three alloys, the density of short rod-like phases in the grain boundary is minimum. According to precipitation morphology and related literatures [1,7], the rod-like phase is β′ phase. The β′ phase acts as an anode and preferentially corrodes during the corrosion process [23]. When a small amount of Ag is added, the density of β″ increases, consequently the mechanical properties of the alloy are improved. However, when excess Ag is added, Ag atoms tend to cluster at grain boundaries and promote the nucleation of the β′ phase.
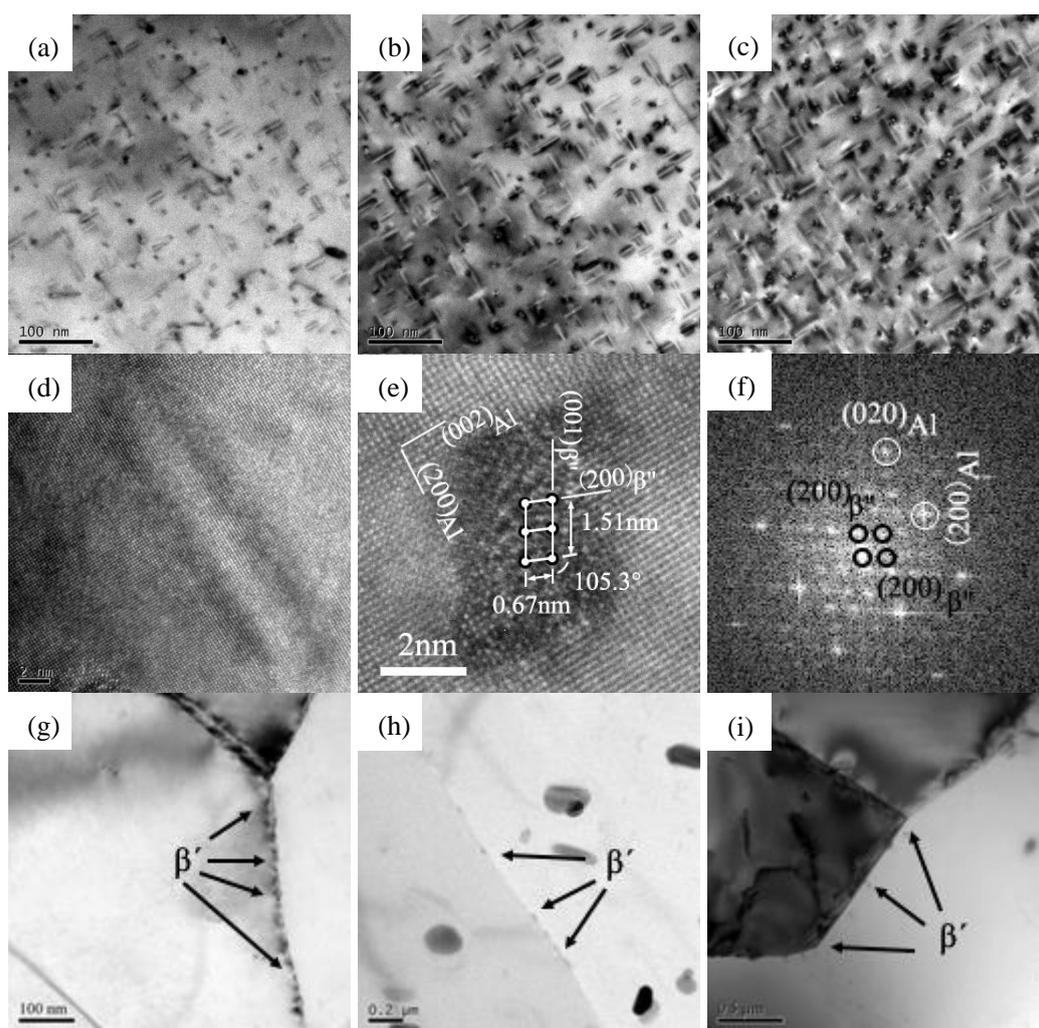


**Figure 4.** TEM images of the alloys with different Ag. (a, g) Alloy A; (b, h) Alloy B; (c, i) Alloy C; (d) HRTEM images of a β″ precipitate and (e, f) the corresponding FFT pattern.

*3.5 DSC*

The kinetic transformation of the precipitation of the Al-Mg-Si alloys with different Ag content

during artificial aging is analyzed, in order to adjust the microstructure and obtain the ideal properties. The DSC curves of the tested alloys at solid solution state are shown in Fig.5. All of the three curves have three endothermic peaks and three exothermic peaks respectively, but the peak intensity and peak position are different. Peak A is suggested to be caused by dissolution of GP zones. Peak B is supposed to be the result of formation of $\beta''$ phase. Peak C is caused by the resolution of $\beta''$ phase. Peak D and peak F is caused by the precipitation of $\beta'$ phase and $\beta$ phase, respectively.

All alloys have a small peak A, indicating that a low level of solute aggregation exists, or that clusters formation during the DSC heating cycle is difficult to dissolve. In addition, no precipitation peak of the clusters is observed on the DSC curves, indicating that atomic aggregation has occurred before the test. As the Ag content increases, the position of peak B  shift the temperature from about 270℃ to 240℃. In addition, the intensity of peak D decreases, which means the suppression precipitation of $\beta'$. In order to obtain the parameters related to the precipitation kinetics of Al-Mg-Si alloy, the JMA equation is used in discussion.
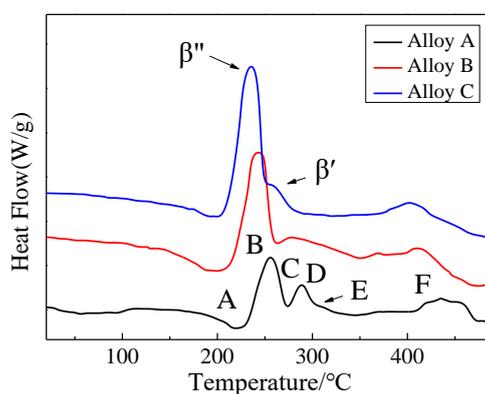


**Figure 5.** DSC curves of the tested alloys

DSC is the differential heat flow value caused by the alloy phase transition at a constant heating rate [24]. Based on these differential calorific value data, the values of the mole fraction (Y) and the precipitation rate (dY/dt) of the precipitated phase can be decided by the computation of the partial area under the reaction curve:

$$Y(T) = \frac{A(T)}{A(T_e)}$$

(A(t) indicates the area covered by the curve between the initial temperature($T_0$) and a given temperature T；A($T_e$) is defined as the area covered by the total curve from the initial temperature to the peak end temperature. The Y(T) values can be derived from different temperatures and the rate of transformed fraction can be identified by [(dY/dT)φ] (dY/dt)) where φ is the constant heating rate (φ = dT/dt). As shown in Fig.5, there are overlaps between the two peaks. In order to facilitate the accurate analysis of the kinetic parameters of the phase, the peak of the main strengthen phase ($\beta''$ and $\beta'$) is selected [1], and the Peakit software is used to separate the overlap peak. The results are shown in Fig. 6.
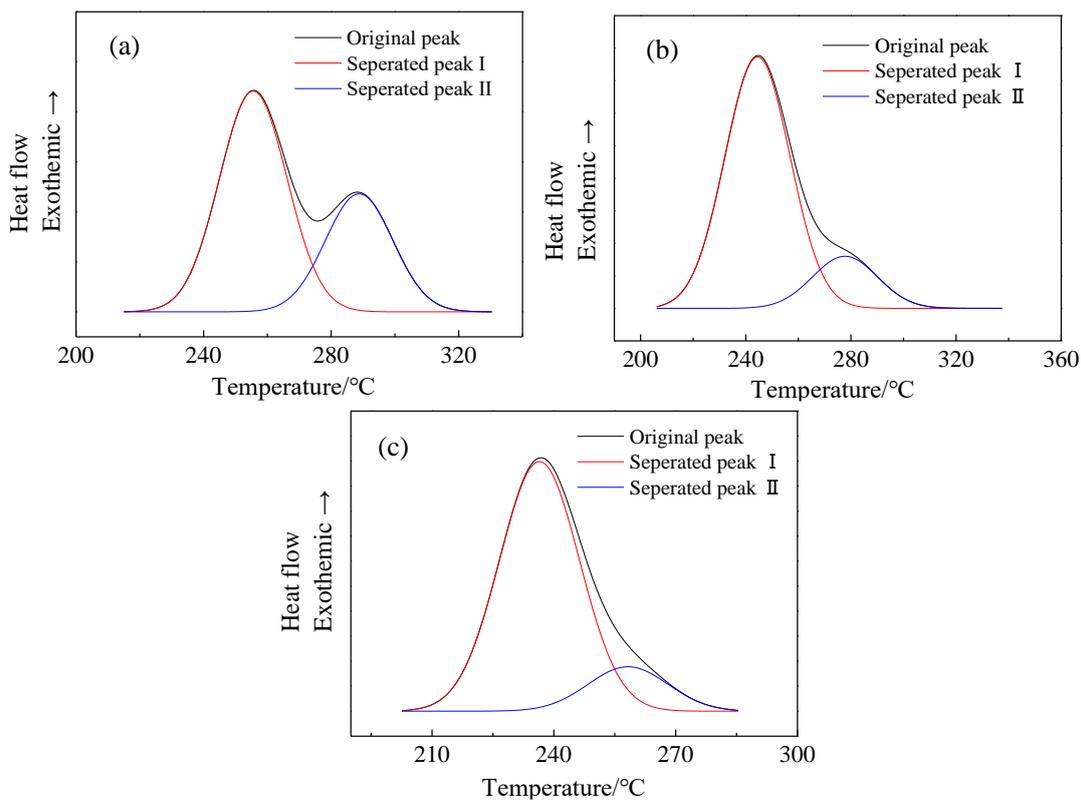
**Figure 6.** Separation results of overlap peak of β" phase and β´phase.(a) Alloy A; (b) Alloy B; (c) Alloy C

According to the separation results of the overlap peak, a typical Y-T relationship curve with S-shaped is obtained (Fig. 7(a)). It can be seen that at the same temperature, the addition of Ag is advantageous for the enhancement of the phase mole fraction of the strengthening phase. In order to obtain the precipitation rate dY/dt of the β" phase and the β´ phase, the temperature of the Y-T curve is derived (Fig. 7(b)). The maximum precipitation rate of β" phase and β´ phase in alloy B and alloy C is higher than that of alloy A. In addition, at the same temperature, the difference of phase precipitation rate between alloy B and alloy C is not obvious.
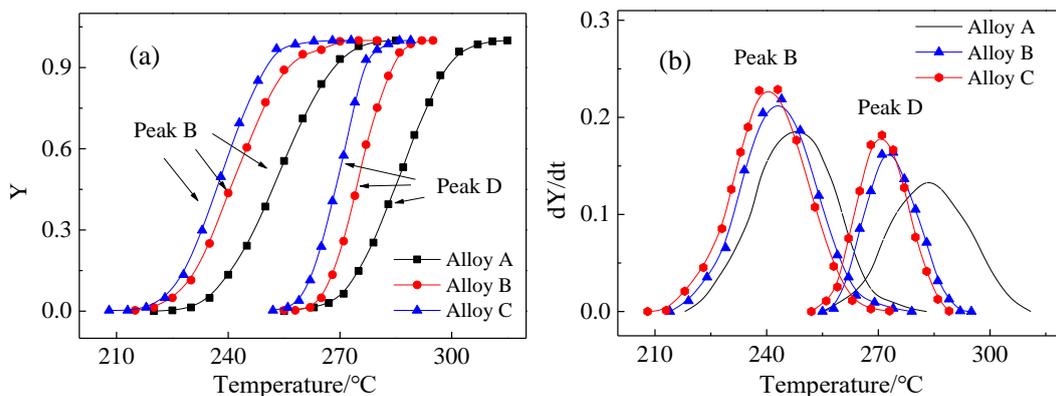


**Figure 7.** Plots of Y vs. T and dY/dt vs. T for the peak of β" phase and β´phase. (a) Plots of Y vs. T for the peak of β" phase and β´phase; (b) Plots of dY/dt vs. T for the peak of β" phase and β´phase

The shift in the peak temperatures with the increasing in Ag content indicates that the reactions are kinetically controlled. For non-isothermal transformation process, a formula was applied to illustrate the rate of the reaction; the rate of reaction can be expressed in the form of [25]:

$$Y = 1 - \exp(-kt^n) \qquad (1)$$

$$k = k_0 \exp(-Q/RT) \qquad (2)$$

Accordingly, the rate of transformation is expressed as following:

$$f(Y) = n(1-Y)[-\ln(1-Y)]^{\frac{n-1}{n}} \qquad (3)$$

$$dY/dt = k^{\frac{1}{n}} f(Y) \qquad (4)$$

Where f(Y) is the implicit function of Y from Eq. (1), $k_0$ is the constant, Q reveals the activation energy, R represent the molar gas constant (= 8.314 J/mol), T is absolute temperature. The values of the parameters k and n are related to the nucleation type and the growth mode. When the precipitation phase is a needle-like precipitation phase, the value of n is 3/2 [25]. Therefore, the following relation can be derived according to the 2, 3, and 4 formulas.

$$\frac{dY}{dT}\varphi = f(Y)k_0 e^{\frac{-Q}{RT}} \qquad (5)$$

Take the logarithm on both sides, Equation 5 can be expressed as:

$$\ln[(\frac{dY}{dT})\varphi] = \ln[f(Y)k_0] - \frac{Q}{R}(\frac{1}{T}) \qquad (6)$$

By formula transformation, Equation 6 can be expressed as:

$$\ln[(\frac{dY}{dT})\varphi/f(Y)] = \ln k_0 - \frac{Q}{R}(\frac{1}{T}) \qquad (7)$$

That is, the precipitation activation energy Q can be determined by the average slope of the linear relationship of ln[(dY/dT)φ/f(Y)] and 1/T. The linear relationship is shown in Figure 8. The relevant parameters are shown in Table 3. The increase in Ag content decreases the activation energy of β" and β′ phase, and accelerates the β" phase precipitation response speed. As shown in Table 3, the activation energy of the β" phase for the alloy A is 105 kJ·mol⁻¹, which is lower than 115 kJ·mol⁻¹ reported in some literatures [26-27]. This result is related to the high content of Mg and Si in the tested alloy. Si can improve the precipitation kinetics of the alloy. When the Ag content increases to 0.6, the activation energy of "β" phase " decreases to 88 kJ·mol⁻¹. At the beginning of aging, Ag atoms have strong binding force with Mg and Si atoms and can replace some Mg atoms as well as form SiAg clusters to increase the cluster density. In the subsequent aging process, added Ag can enhance the aging response speed of the β" phase, and increase the density of β" phase. In addition, it can be deduced that the addition of Ag can inhibit the transformation from β"phase to β′ phase and enhance the thermodynamic stability of the β"phase [28].
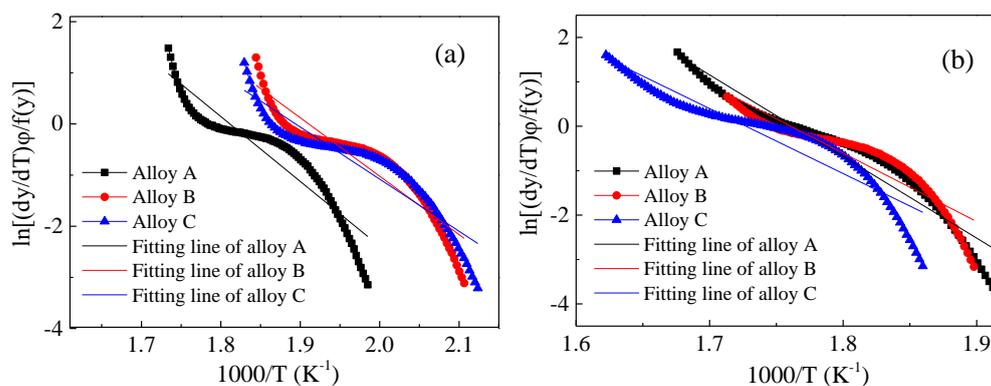
**Figure 8.** Plots of ln[(dY/dT)φ] vs. (1/T) for given Y values to determine the kinetic parameters of the β″ and β′exothermic peaks of the three Alloys. (a) β″ phase exothermic peak; (b) β′exothermic peak

**Table 3.** Kinetic parameters for β″ and β′ peaks of the three alloys

| Alloy | $Q_{β''}$/kJ·mol$^{-1}$ | $Q_{β'}$/kJ·mol$^{-1}$ | n |
|-------|-------------------------|------------------------|-----|
| A | 105.452 | 152.807 | 1.5 |
| B | 94.9927 | 128.128 | 1.5 |
| C | 88.7252 | 122.656 | 1.5 |

For Al-Mg-Si alloys, the surface state is critical to the performance of the alloy in corrosive environment. The continuity of grain boundary precipitates is also an important factor with regard to whether can be corroded deep into the alloy. The continuous precipitations (β′) of the grain boundary as an anodic corrosion channel accelerate the corrosion process. The specific corrosion process has been reported in related literatures.[1)]

Compared to Alloy A, the density of the grain boundary precipitation (β′) of the alloy B is lower. As well alloy B has intermittent grain boundary precipitation phase, which can cut off the anode corrosion channel and improve the corrosion resistance. When the Ag content in the alloy increases to 0.6 wt.%, the density of grain boundary (β′) increases, leading to an increase inIGC depth. Maloney believes that Ag has a strong ability of adsorption with Mg and Si atoms during aging, which shows strong ability to form AgMgSi cluster.[13] These clusters act as β″ nucleation sites in the subsequent aging process to increase the density of the strengthen phase. When the alloy is added with excess Ag, the enriched Ag at the grain boundary increases the density of the β′ phase, which reduces the corrosion resistance of the alloy. Therefore, the addition of a small amount of Ag is beneficial to improve the overall performance of the alloy.

## 4. CONCLUSIONS

The addition of Ag can significantly accelerate the age-hardening rate, effectively increase the density of the β″ strengthening phase of the Al-Mg-Si alloys, and, decreases its softening rate. The precipitation activation energy of β″ and β′ decreases with the increase in Ag content. The activation

energy values are 105, 94, 88 kJ/mol and 152, 128, 122 kJ/mol, respectively.

The corrosion resistance of the alloy initially increases and then decreases with the increase of Ag content. The alloy without Ag presents severe localized corrosion andIGC; the alloy with 0.3% Ag content has fewer β′ anode phases on the grain boundary and exhibits a slight IGC. The increasing density of β′ phase and the enhancing corrosion sensitivity of the alloy can be ascribed to the added excessive Ag.

## References

1.  Y.Y. Zheng, B. Luo, Z. Bai, J. Wang and Y. Yin, *Metals*, 7(2017) 387.
2.  C. Flament, J. Ribis, J. Garnier, Y. Serruys, F. Leprêtre, A. Gentils, C. Baumier, M. Descoins, D. Mangelinck, A. Lopez, K. Colas, K. Buchanan, P. Donnadieu and A, Deschamps, *Acta Mater.*, 128(2017) 64.
3.  G.A. Edwards, K. Stiller, G.L. Dunlop and M.J. Couper, *Acta Mater.,* 46(1998) 3893.
4.  V. Fallah, B. Langelier, N. Ofori-Opoku, B. Raeisinia, N. Provatas and S. Esmaeili, *Acta Mater.*, 103(2016) 290.
5.  S. J. Andersen, H.W. Zandbergen, J. Jansen, C. Traeholt, U. Tundal and O. Reiso, *Acta Mater.*, 46(1998) 3283.
6.  J.H. Chen, E. Costan, M.A. Vanhuis, Q. Xu and H.W. Zandbergen, *Science*, 312(2006) 416.
7.  L. Cao, A. Paul, Rometsch, J. Malcolm and Couper, *Mater. Sci. Eng.*, A, 559(2013) 257.
8.  A. Gaber, A. Mossad Ali, K. Matsuda, T. Kawabata, T. Yamazaki and S. Ikeno, *J. Alloys Compd.*, 432(2007) 149.
9.  J.H. Kim, C.D. Marioara, R. Holmestad, E. Kobayashi and T. Sato, *Mater. Sci. Eng*. A, 560(2013) 154.
10. W. Yuan and Z. Liang, *Mater. Des.*, 32(2011) 4195.
11. L. Ding, Z. Jia, Z. Zhang, R. E. Sanders, Q. Liu and G. Yang, *Mater. Sci. Eng*. A, 627(2015) 119.
12. C.D Marioara, S.J Andersen, J Jansen and H.W Zandbergen, *Acta Mater.*, 51(2003) 789.
13. J. Nakamura, K. Matsuda, T. Kawabata, T. Sato, Y. Nakamura and S. Ikeno, *Mater. Trans.*, 51(2010) 310.
14. C. Cayron and P. A. Buffat, *Acta Mater.*, 48(2000) 2639.
15. T. Ishizaki, Y. Masuda, M. Sakamoto, A. Shimo and M. Nagoya, *Langmuir*, 27(2011) 4780.
16. M. Tokuda, K. Matsuda, T. Nagai, T. Kawabata, J. Nakamura and S. Ikeno, *Arch. Metall. Mater.*, 58(2013) 363.
17. Y, Weng, Z. Jia, L. Ding, Y. Pan, Y. Liu and Q. Liu, *J. Alloys Compd.*, 695(2017) 2444.
18. O.M. John, Bockris áá and Y. Kang, *J. Solid State Electrochem.*, 1(1997) 17.
19. A. Earl and Gulbransena, *J. Electrochem. Soc.*, 91(1947) 573.
20. U.D.Rameez, Visweswara C. Gudla, S. Morten, Jellesen and A, Rajan, *Surf. Coat. Technol.*, 276(2015) 77.
21. E. McCafferty, *Corros. Sci.*, 45(2003) 301.
22. J.C.S. Fernandes, R. Picciochi, M.D. Belo, T.M. Silva, M. G. S. Ferreira and I. T. E. Fonseca, *Electrochim. Acta*, 49(2004) 4701.
23. Z. Li, C. Li, Z. Gao, Y. Liu, X. Liu, Q. Guo, L. Yu and H. Li, *Mater. Charact.*, 110(2015) 170.

24. K.A.Q. Reilly and B. Cantor, *Proc. R. Soc. London, Ser.* A, 452(1996) 2141.
25. C. Fatih, *J. Alloy Compd.*, 623(2015) 184.
26. R.S. Yassar, D.P. Field, and H. Weiland, *Metall. Mater. Trans.* A, 36(2005) 2059.
27. Q. Zhao, X. Yuan, H. Huang and P. Zhao, *Rare Metal Mat. Eng.*, 11(2016) 2889
28. S. Jin, T. Ngai, G. Zhang, T. Zhai, S. Jia and L. Li, *Mater. Sci. Eng.,* A, 724(2018) 53.